GEOLOGY | THE GEOLOGICAL SOCIETY OF AMERICA®

https://doi.org/10.1130/G49714.1

Manuscript received 15 April 2021
Revised manuscript received 15 September 2021
Manuscript accepted 18 January 2022

Published online 11 April 2022

Five million years of high atmospheric CO_2 in the aftermath of the Permian-Triassic mass extinction

Michael M. Joachimski[1]*, Johann Müller[1], Timothy M. Gallagher[2], Gregor Mathes[3], Daoliang L. Chu[4], Fedor Mouraviev[5], Vladimir Silantiev[5], Yadong D. Sun[1] and Jinnan N. Tong[4]

[1]GeoZentrum Nordbayern, Friedrich-Alexander Universität Erlangen-Nürnberg (FAU), Erlangen 91054, Germany
[2]Department of Geology, Kent State University, Kent, Ohio 44240, USA
[3]Department of Sport Science & Bayreuth Center of Ecology and Environmental Research (BayCEER), Universität Bayreuth, Bayreuth 95447, Germany
[4]State Key Laboratory of Biogeology and Environmental Geology, School of Earth Sciences, China University of Geosciences, Wuhan 430074, China
[5]Geology and Petroleum Technologies, Kazan Federal University, 420008 Kazan, Russia

ABSTRACT

The end-Permian mass extinction, the largest biological crisis in Earth history, is currently understood in the context of Siberian Traps volcanism introducing large quantities of greenhouse gases to the atmosphere, culminating in the Early Triassic hothouse. In our study, the late Permian and Early Triassic atmospheric CO_2 history was reconstructed by applying the paleosol pCO_2 barometer. Atmospheric pCO_2 shows an approximate 4× increase from mean concentrations of 412–919 ppmv in the late Permian (Changhsingian) to maximum levels between 2181 and 2610 ppmv in the Early Triassic (late Griesbachian). Mean CO_2 estimates for the later Early Triassic are between 1261–1936 ppmv (Dienerian) and 1063–1757 ppmv (Spathian). Significantly lower concentrations ranging from 343 to 634 ppmv are reconstructed for the latest Early to Middle Triassic (Anisian). The 5 m.y. episode of elevated pCO_2 suggests that negative feedback mechanisms such as silicate weathering were not effective enough to reduce atmospheric pCO_2 to precrisis levels and that marine authigenic clay formation (i.e., reverse weathering) may have been an important component of the global carbon cycle keeping atmospheric pCO_2 at elevated levels.

INTRODUCTION

The end-Permian mass extinction (ca. 252 Ma) coincided with the onset of intrusive Siberian Traps volcanism, which was likely responsible for outgassing of large quantities of CO_2, CH_4, and halogens by thermogenic heating of volatile-rich sediments (Courtillot and Renne, 2003; Svensen et al., 2009; Burgess and Bowring, 2015). The inferred increase in greenhouse gas concentrations has been interpreted to have resulted in a dramatic 8–10 °C increase in low-latitude sea-surface temperature (SST), with high ocean temperatures persisting into the Early Triassic (e.g., Sun et al., 2012; Joachimski et al., 2020). However, a proxy record for atmospheric pCO_2 has yet to be established for the late Permian to Early Triassic.

We reconstructed the late Permian to Middle Triassic atmospheric CO_2 record by applying the carbonate paleosol pCO_2 barometer to soil carbonates from sections in northwest China (Xinjiang Province), north China (Henan and Shanxi Provinces), Russia (South Ural foreland basin), South Africa (Karoo Basin), and the United Kingdom (Dorset) (Fig. 1; Table S1 in the Supplemental Material[1]). Stratigraphically, the samples cover the Changhsingian (late Permian) to earliest Griesbachian, late Griesbachian to Dienerian, and Spathian to Anisian (Early to Middle Triassic). Reconstructed atmospheric CO_2 levels suggest an approximate 4-fold increase in pCO_2 from the latest Permian to Early Triassic, high to intermediate CO_2 levels in the Early Triassic, and a decline to precrisis levels in the latest Early Triassic.

PALEOSOL pCO_2 BAROMETER

We calculated atmospheric CO_2 concentrations from the carbon isotopic composition of microsampled micritic soil carbonate precipitated in the well-drained soils by applying a two-component carbon isotope mixing model, given that soil CO_2 is a mixture of two isotopically different CO_2 sources (soil-respired CO_2 and atmospheric CO_2; Cerling, 1991):

$$\left[CO_2\right]_{atm} = S(z) \times \frac{(\delta^{13}C_s - 1.0044 \times \delta^{13}C_{resp} - 4.4)}{\delta^{13}C_{atm} - \delta^{13}C_s}. \quad (1)$$

Here, $S(z)$ is the soil-derived (respired) component of total soil CO_2, and $\delta^{13}C_s$, $\delta^{13}C_{resp}$, and $\delta^{13}C_{atm}$ represent the carbon isotopic compositions of total soil CO_2, soil-respired CO_2, and atmospheric CO_2, respectively. The $\delta^{13}C_s$, $\delta^{13}C_{resp}$, and $\delta^{13}C_{atm}$ values were calculated from the measured $\delta^{13}C$ value of pedogenic carbonate, soil organic matter (SOM) occluded in the carbonate nodules, and marine carbonate, respectively.

The soil-derived contribution of CO_2, $S(z)$, and the soil temperature must be assumed, presenting the main uncertainties for paleo-pCO_2 reconstructions. While earlier studies used high $S(z)$ values of 5000 ppmv (e.g., Ekart et al., 1999), representing soil CO_2 concentrations of the mean growing season, later studies observed that pedogenic carbonate precipitation mainly occurs during warm and dry periods characterized by a relatively low soil pCO_2 due to moisture-limited soil respiration (Breecker et al.,

*E-mail: michael.joachimski@fau.de

[1]Supplemental Material. Detailed description of locations, samples, and methods, Figures S1–S3, and Tables S1–S4. Please visit https://doi.org/10.1130/GEOL.S.19386206 to access the supplemental material, and contact editing@geosociety.org with any questions.

CITATION: Joachimski, M.M., et al., 2022, Five million years of high atmospheric CO_2 in the aftermath of the Permian-Triassic mass extinction: Geology, v. 50, p. 650–654, https://doi.org/10.1130/G49714.1

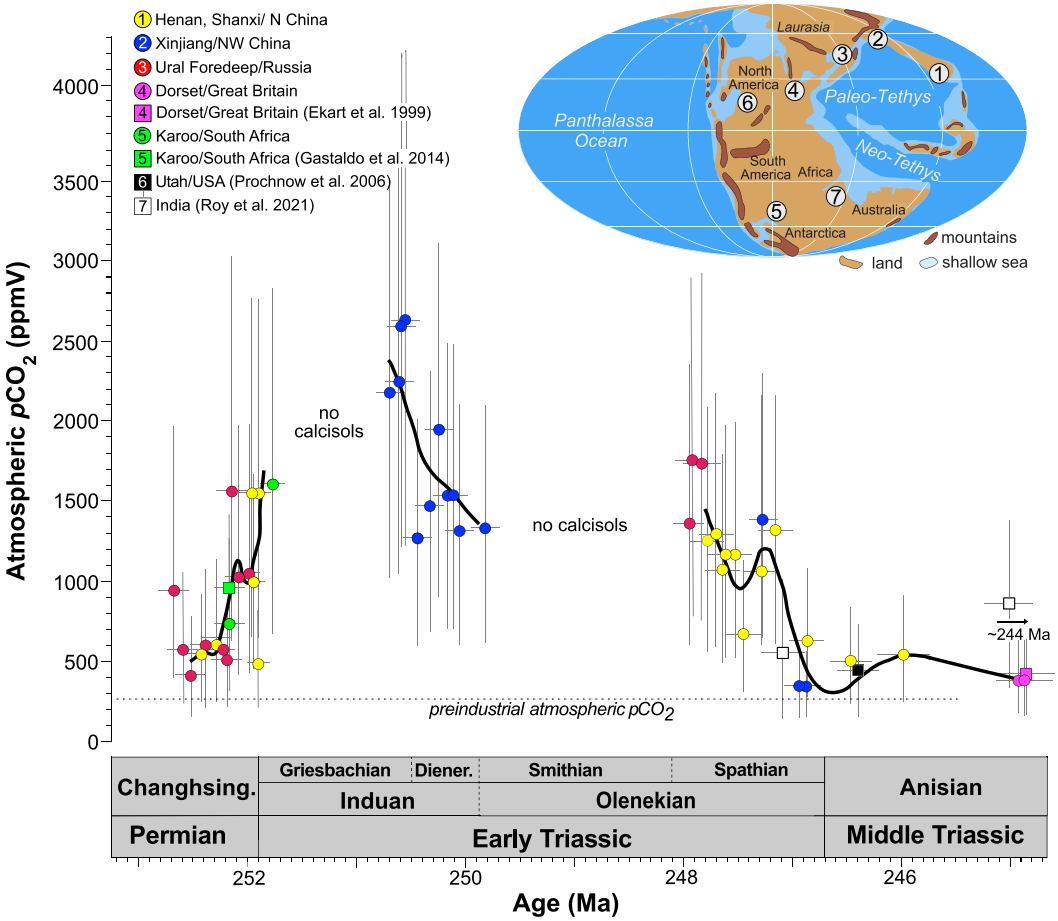

Figure 1. The Permian-Triassic atmospheric CO_2 record. Symbols represent mean values of atmospheric pCO_2 calculated based on the distribution of all possible values by varying soil temperature (*T*), soil-respired CO_2 concentration [*S*(z)], and $\delta^{13}C$ of atmospheric CO_2. Vertical bars are 95% credible intervals for each estimate, calculated using quantile intervals of distribution of all possible values of each sample. Horizontal bars give sample age uncertainties. Trend line represents the Locfit (https://cran.r-project.org/web/packages/locfit/index.html) regression (α = 0.6). Stratigraphic scheme and absolute ages are according the Geological Time Scale 2020 (Ogg and Chen, 2020). Permian-Triassic paleogeographic reconstruction with study locations after Scotese and Moore (2014). Changhsing—Changhsingian; Diener—Dienerian.

2009). We assumed *S*(z) values between 500 and 1500 ppmV following Montañez (2013), who used the $\delta^{13}C$ difference between modern soil carbonate and SOM ($\Delta_{carb\text{-}org}$) to constrain *S*(z) for different soil orders (see the Supplemental Material for details).

Soil temperature has to be estimated in order to calculate $\delta^{13}C_{resp}$ from the $\delta^{13}C$ value of pedogenic carbonate, utilizing the temperature-dependent carbon isotope fractionation between CO_2 and CO_3^{2-} (Romanek et al., 1992). Soil temperatures for the calcisols formed at various paleolatitudes were estimated using low-latitude SSTs (Sun et al., 2012; Joachimski et al., 2020), a low-latitudinal temperature gradient for warm climatic conditions (0.2 °C per 1° latitude; Zhang et al., 2019), air temperatures 3 °C lower than SSTs (Zhang et al., 2019), and 2–4 °C warmer soil temperatures compared to atmospheric temperatures (Hu and Feng, 2003; Table S2).

Atmospheric pCO_2 was calculated for each possible combination of *S*(z), soil temperature (Table S2), and $\delta^{13}C$ of atmospheric CO_2 (Table S3) by varying *S*(z) from 500 to 1500 ppmv in 100 ppm steps, increasing soil temperature in 1 °C steps (using a ±5 °C temperature range around estimated average soil temperature), and $\delta^{13}C$ of atmospheric CO_2 in 0.1‰ steps. Mean atmospheric CO_2 concentrations for each sample were then calculated based on the distribution of all possible values. The 95% credible interval (CI) for each estimate and sample was calculated using the quantile intervals (95% CI [lower quantile, upper quantile]) of the distribution of all possible values of each sample (Table S4).

RESULTS

Studied Paleosols

All studied paleosols were classified as Calcisols because they are characterized by rare to common carbonate nodules (up to several centimeters in size; stage II nodules) or layers with stacked carbonate nodules and rhizocretions (stage II; Fig. S1). Of a total of 105 pedogenic carbonate samples, 46 carbonates showed characteristic pedogenic features (Fig. S2) as well as carbon isotope values indicative of carbonate precipitation under the influence of atmospheric CO_2, and these were accepted as having formed in the nonsaturated zone and used for atmospheric pCO_2 reconstruction (see the Supplemental Material).

Permian–Triassic Atmospheric pCO_2

Mean atmospheric pCO_2 showed a significant increase from the latest Permian (Changhsingian) to Early Triassic, with elevated pCO_2 persisting until the latest Early Triassic (Fig. 1). Late Changhsingian mean atmospheric pCO_2 estimates derived from Russian, North China, and Karoo samples are generally between 412 (95% CI [162, 688]) and 949 ppmv (95% CI [400, 1743]; $n = 9$). Atmospheric CO_2 started to increase before the Permian-Triassic boundary (PTB) to levels between 1031 ppmv (95% CI [419, 1966]) and 1558 ppmv (95% CI [676, 2789]; $n = 6$). Sample PY2 (north China) yielded a lower atmospheric CO_2 content of 483 ppmv (95% CI [214, 833]). In the earliest Griesbachian, the mean pCO_2 was at 1606 ppmv (95% CI [689, 2919]). Atmospheric pCO_2 in the late Griesbachian (Xinjiang) ranged from 2181 (95% CI [1025, 3516]) to 2610 ppmv (95% CI [1224, 4226]; $n = 4$), being on average 4× higher than Changhsingian background levels. Estimates for the Dienerian (Xinjiang) are between 1261 (95% CI [596, 2009]) and 1936 ppmv (95% CI [921, 3104]; $n = 6$), while estimates for the Spathian paleosols (Russia, North China, and Xinjiang) range from 1063 (95% CI [490, 1765]) to 1757 ppmv (95% CI [792, 2994]; $n = 11$), except sample DYLY, which yielded a CO_2 concentration of 671 ppmv (95% CI [306, 1124]). Terminal hothouse (latest Spathian and Anisian) pCO_2 estimates based on paleosols from Xinjiang, North China, and the United Kingdom are between 343 (95% CI [155, 575]) and 634 ppmv (95% CI [285, 1067]; $n = 6$), i.e., considerably

lower than most Early Triassic pCO_2 estimates but comparable to Changhsingian CO_2 levels.

DISCUSSION

The atmospheric pCO_2 estimates are in good agreement with published pCO_2 reconstructions from paleosol nodules (Karoo Basin—Gastaldo et al., 2014; India—Roy et al., 2021), stomatal index data (Li et al., 2019; Retallack and Conde, 2020), and in part with estimates based on C_3 plant carbon isotope fractionation (Wu et al., 2021; Fig. 2). However, the reliability of this latter method is controversial (e.g., Lomax et al., 2019). This could explain the significant drop in pCO_2 above the PTB reconstructed by Wu et al. (2021), which is at odds with increasing low-latitude SSTs as well as high Dienerian and Spathian pCO_2 values (this study; Fig. 2). Published Anisian paleosol pCO_2 estimates were recalculated (Fig. 1), as they had originally been calculated with S(z) of up to 5000 ppmv (Ekart et al. 1999; Prochnow et al. 2006). Most importantly, the generally good agreement among pCO_2 estimates reconstructed from time-equivalent paleosols from distant sites (this study; Fig. 1) and the comparable estimates derived from other CO_2 proxies (Fig. 2) underline the validity of the atmospheric CO_2 record presented here. However, the evolution of atmospheric pCO_2 during most of the Griesbachian and the Smithian remains unresolved because no suitable pedogenic carbonates have been found for these periods.

Early Triassic Greenhouse

Siberian Traps volcanism is interpreted as a proximate cause of the 4× increase in atmospheric CO_2 from the latest Permian (Changhsingian) to Early Triassic (late Griesbachian). The onset of Siberian effusive volcanism has been dated prior to 252.2 ± 0.1 Ma (Burgess and Bowring, 2015), ~300 k.y. before the end-Permian mass extinction. Subsequent intrusive magmatism starting at 251.9 ± 0.067 Ma probably produced >100.000 GT of CO_2 and CH_4 by thermogenic heating of sediments around large sill intrusions (Svensen et al., 2009; Augland et al., 2019). This massive emission of greenhouse gases (depleted in ^{13}C) has been suggested as the main cause of dramatic global warming, as well as of the negative carbon isotope excursion recorded globally in the latest Changhsingian to early Griesbachian (Fig. 2).

Parallel to the reconstructed rise in atmospheric pCO_2 from 412–949 ppmv in the latest Changhsingian to 2181–2610 ppmv in the late Griesbachian, low-latitude SSTs calculated from oxygen isotopes measured on conodont apatite (Fig. 2) increased by 7–10 °C, from 25–28 °C to >35 °C (Joachimski et al., 2020). With the decrease in pCO_2 in the late Spathian to Anisian, SSTs decreased again (Sun et al., 2012; Fig. 2). Thus, pCO_2 as well as SSTs persisted at high levels for almost 5 m.y. (Fig. 2), representing an unusually long time interval. High atmospheric pCO_2 conditions could only be sustained either by continuous and massive CO_2 outgassing from Siberian Traps or by reduced CO_2 consumption by continental silicate weathering and biological uptake. The emplacement of large volumes of subvolcanic intrusions (sills and dikes) started in the latest Changhsingian but continued for only 0.5 m.y. into the Early Triassic (Augland et al., 2019; Burgess and Bowring, 2015). Although large igneous province volcanism has been reported to have been active until the end of the Middle Triassic (Ivanov, 2007), published geochronological data have large uncertainties of ~5 m.y. and cannot resolve whether contact metamorphism resulted in prolonged degassing after the initial violent pulse (Augland et al., 2019). Notably, Hg concentrations in marine carbonates argue for massive volcanic activity at the Permian-Triassic transition, in accord with the Siberian Traps record, but for reduced volcanic emissions in the later Early Triassic (Wang et al., 2018).

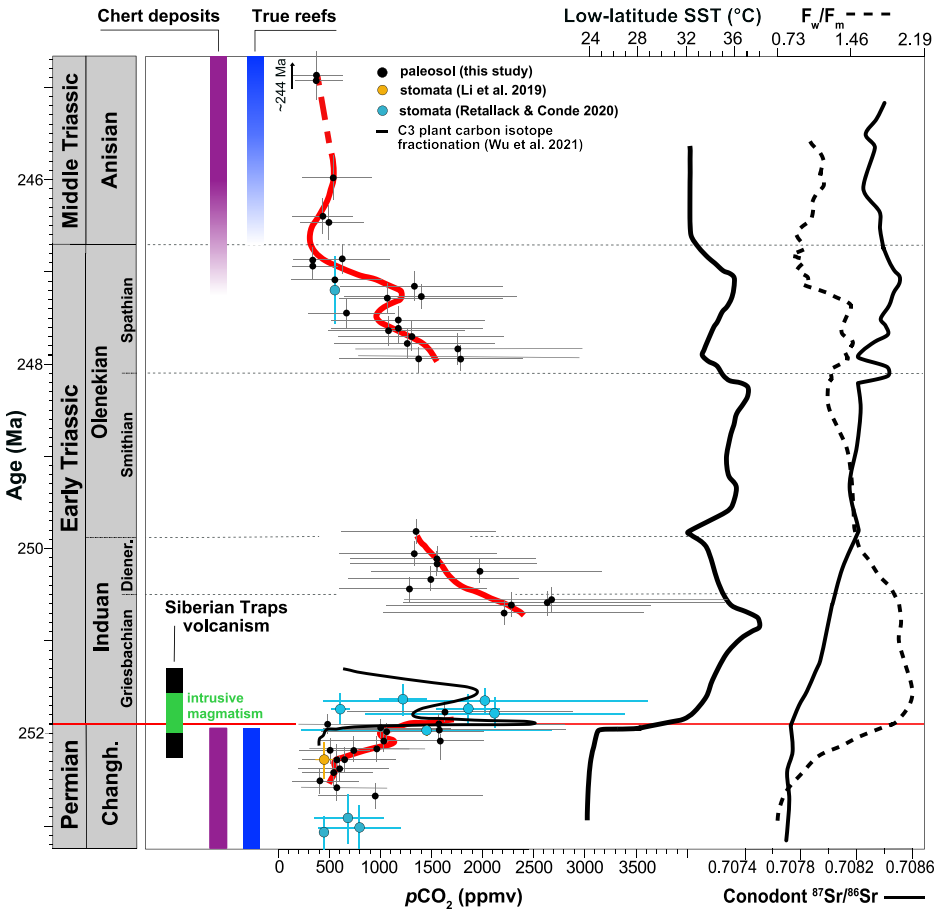

Figure 2. Comparison of Permian-Triassic atmospheric pCO_2 estimates, low-latitude sea-surface temperature (SST; Sun et al., 2012; Joachimski et al., 2020), conodont $^{87}Sr/^{86}Sr$, and modeled ratio of terrestrial Sr (F_w) versus mantle Sr (F_m) flux (Song et al., 2015). Red trend line represents the Locfit (https://cran.r-project.org/web/packages/locfit/index.html) regression (α = 0.6) for mean paleosol pCO_2 estimates. Note the relatively good correspondence among pCO_2, SST, and modeled F_w/F_m, suggesting that although continental weathering increased, atmospheric pCO_2 and SSTs stayed at high levels. Siberian Traps volcanism is from Burgess and Bowring (2015). Changh—Changhsingian; Diener—Dienerian. Chert and reef record modified after Chen and Benton (2012).

Early Triassic Atmospheric pCO_2 Regulated by Weathering

Assuming that the outgassing of large volumes of volcanic CO_2 faded after the initial 0.5-m.y.-long phase, atmospheric pCO_2 is expected to have been drawn down relatively fast by continental silicate weathering—the most effective mechanism by which to extract CO_2 from the atmosphere and to buffer Earth's climate. However, pCO_2 stayed at elevated levels for ~4 m.y. after the Griesbachian CO_2 maximum.

Warm temperatures, water availability, and continental plates located within the humid climatic belt are the main factors favoring silicate weathering. Weathering of freshly deposited continental flood basalts would have been particularly effective at consuming atmospheric CO_2, with weathering rates of basalts being 10 times greater compared to weathering rates of

granitic continental rocks (Dessert et al., 2003). This efficiency has been documented for Late Triassic Central Atlantic Magmatic Province (CAMP) volcanism, when individual volcanic pulses resulted in a doubling of atmospheric pCO_2 followed by a striking decrease to pre-eruption levels within only ~300 k.y. (Schaller et al., 2012). While CAMP volcanism occurred in warm equatorial latitudes favorable for CO_2 consumption by silicate weathering, the Siberian Traps erupted at ~60°N, with silicate weathering potentially less efficient due to colder conditions. However, the latest Permian increase of low-latitude SSTs likely resulted in an amplified warming of higher latitudes. In conjunction with intensified higher-latitude precipitation as suggested by climate modeling (Winguth et al., 2015), weathering of freshly deposited Siberian lavas should have had the potential to consume atmospheric CO_2. In contrast, Kump (2018) argued that low continental fragmentation and high continentality in Pangea's interiors combined with minimum uplift rates depressed CO_2 uptake by silicate weathering. However, this interpretation seems to be at odds with strontium as well as osmium isotope records (Song et al., 2015; Liu et al., 2020), which indicate an increase in continental weathering, especially in the Early Triassic (Fig. 2).

Silicate weathering can be modulated by reverse weathering, whereby non-kaolinite phyllosilicates form on the seafloor, leading to consumption of dissolved silica and alkalinity sourced from weathering on land and, most important, the addition of CO_2 to the ocean-atmosphere system (Isson and Planavsky, 2018). Reverse weathering has been suggested as a mechanism to maintain high pCO_2 in the Precambrian, when oceans were probably characterized by high dissolved silica concentrations (Maliva et al., 2005) before the advent of silica-secreting organisms. Interestingly, while the Permian is known for extensive chert deposition, cherts disappeared almost completely from the rock record in the Early Triassic (Beauchamp and Baud, 2002). A low abundance of silica-secreting organisms, warm ocean temperatures (increasing silica solubility), and supply of silica from land probably led to high dissolved silica concentrations in Early Triassic oceans, which should have promoted reverse weathering. Cherts re-occurred in the Spathian and Anisian (Sperling and Ingle, 2006) in conjunction with the diversification of radiolarians (O'Dogherty et al., 2010) and the late Spathian decrease in pCO_2.

In summary, the 4× increase in atmospheric pCO_2 across the Permian-Triassic boundary to high and intermediate CO_2 levels in the Early Triassic is in agreement with low-latitude SSTs documenting greenhouse warming and hot Early Triassic oceans. Elevated atmospheric pCO_2 persisted for ~5 m.y., suggesting that warm-climate–enhanced silicate weathering, although indicated by geochemical proxies, failed to draw down CO_2 until the latest Early Triassic. This apparent contradiction may indicate that the exceptional conditions in Early Triassic oceans led to an intensification of marine authigenic clay formation and contribution of CO_2 to the ocean-atmosphere system, counteracting CO_2 consumption by silicate weathering.

ACKNOWLEDGMENTS

Financial support by the National Natural Science Foundation of China (grant 41821001) is acknowledged. V. Silantiev and F. Mouraviev were supported by a subsidy allocated to Kazan Federal University (Russia) for the state assignment 671–2020–0049 in the sphere of scientific activities and cont. no. 14.Y26.31.0029, res. no. 220 of the Government of the Russian Federation. Helpful comments by anonymous reviewers on an earlier version of this manuscript are acknowledged. This is a contribution to Deutsche Forschungsgemeinschaft (DFG) Research Unit TERSANE (FOR 2332: Temperature-related stressors as a unifying principle in ancient extinctions; project Jo 219/15–1).

REFERENCES CITED

Augland, L.E., Ryabov, V.V., Vernikovsky, V.A., Planke, S., Polozov, A.G., Callegaro, S., Jerram, D.A., and Svensen, H.H., 2019, The main pulse of the Siberian Traps expanded in size and composition: Scientific Reports, v. 9, p. 18723, https://doi.org/10.1038/s41598-019-54023-2.

Beauchamp, B., and Baud, A., 2002, Growth and demise of Permian biogenic chert along northwest Pangea: Evidence for end-Permian collapse of thermohaline circulation: Palaeogeography, Palaeoclimatology, Palaeoecology, v. 184, p. 37–63, https://doi.org/10.1016/S0031-0182(02)00245-6.

Breecker, D.O., Sharp, Z.D., and McFadden, L.D., 2009, Seasonal bias in the formation and stable isotopic composition of pedogenic carbonate in modern soils from central New Mexico, USA: Geological Society of America Bulletin, v. 121, p. 630–640, https://doi.org/10.1130/B26413.1.

Burgess, S.D., and Bowring, S.A., 2015, High-precision geochronology confirms voluminous magmatism before, during, and after Earth's most severe extinction: Science Advances, v. 1, e1500470, https://doi.org/10.1126/sciadv.1500470.

Cerling, T.E., 1991, Carbon dioxide in the atmosphere: Evidence from Cenozoic and Mesozoic paleosols: American Journal of Science, v. 291, p. 377–400, https://doi.org/10.2475/ajs.291.4.377.

Chen, Z.-Q., and Benton, M.J., 2012, The timing and pattern of biotic recovery following the end-Permian mass extinction: Nature Geoscience, v. 5, p. 375–383, https://doi.org/10.1038/ngeo1475.

Courtillot, V.E., and Renne, P.R., 2003, On the ages of flood basalt events: Comptes Rendus Geoscience, v. 335, p. 113–140, https://doi.org/10.1016/S1631-0713(03)00006-3.

Dessert, C., Dupré, B., Gaillardet, J., François, L.M., and Allègre, C.J., 2003, Basalt weathering laws and the impact of basalt weathering on the global carbon cycle: Chemical Geology, v. 202, p. 257–273, https://doi.org/10.1016/j.chemgeo.2002.10.001.

Ekart, D.D., Cerling, T.E., Montanez, I.P., and Tabor, N.J., 1999, A 400 million year carbon isotope record of pedogenic carbonate: Implications for paleoatmospheric carbon dioxide: American Journal of Science, v. 299, p. 805–827, https://doi.org/10.2475/ajs.299.10.805.

Gastaldo, R.A., Knight, C.L., Neveling, J., and Tabor, N.J., 2014, Latest Permian paleosols from Wapadsberg Pass, South Africa: Implications for Changhsingian climate: Geological Society of America Bulletin, v. 126, p. 665–679, https://doi.org/10.1130/B30887.1.

Hu, Q., and Feng, S., 2003, A daily soil temperature dataset and soil temperature climatology of the contiguous United States: Journal of Applied Meteorology, v. 42, p. 1139–1156, https://doi.org/10.1175/1520-0450(2003)042<1139:ADSTDA>2.0.CO;2.

Isson, T.T., and Planavsky, N.J., 2018, Reverse weathering as a long-term stabilizer of marine pH and planetary climate: Nature, v. 560, p. 471–475, https://doi.org/10.1038/s41586-018-0408-4.

Ivanov, A.V., 2007, Evaluation of different models for the origin of the Siberian Traps, *in* Foulger, G.R., and Jurdy, D.M., eds., Plates, Plumes, and Planetary Processes: Geological Society of America Special Paper 430, p. 669–691, https://doi.org/10.1130/2007.2430(31).

Joachimski, M.M., Alekseev, A.S., Grigoryan, A., and Gatovsky, Yu.A., 2020, Siberian Trap volcanism, global warming and the Permian-Triassic mass extinction: New insights from Armenian Permian-Triassic sections: Geological Society of America Bulletin, v. 132, p. 427–443, https://doi.org/10.1130/B35108.1.

Kump, L.R., 2018, Prolonged late Permian–Early Triassic hyperthermal: Failure of climate regulation: Philosophical Transactions Royal Society, series A, v. 376, p. 20170078, https://doi.org/10.1098/rsta.2017.0078.

Li, H., Yu, J., McElwain, J.C., Yiotis, C., and Chen, Z.Q., 2019, Reconstruction of atmospheric CO_2 concentration during the late Changhsingian based on fossil conifers from the Dalong Formation in South China: Palaeogeography, Palaeoclimatology, Palaeoecology, v. 519, p. 37–48, https://doi.org/10.1016/j.palaeo.2018.09.006.

Liu, Z., Selby, D., Zhang, H., and Shen, S.-Z., 2020, Evidence for volcanism and weathering during the Permian-Triassic mass extinction from Meishan (South China) osmium isotope record: Palaeogeography, Palaeoclimatology, Palaeoecology, v. 553, p. 109790, https://doi.org/10.1016/j.palaeo.2020.109790.

Lomax, B.H., Lake, J.A., Leng, M.J., and Jardine, P.E., 2019, An experimental evaluation of the use of $\Delta^{13}C$ as a proxy for palaeoatmospheric CO_2: Geochimica et Cosmochimica Acta, v. 247, p. 162–174, https://doi.org/10.1016/j.gca.2018.12.026.

Maliva, R.G., Knoll, A.H., and Simonson, B.M., 2005, Secular change in the Precambrian silica cycle: Insights from chert petrology: Geological Society of America Bulletin, v. 117, p. 835–845, https://doi.org/10.1130/B25555.1.

Montañez, I.P., 2013, Modern soil constraints on reconstructing deep-time atmospheric CO_2: Geochimica et Cosmochimica Acta, v. 101, p. 57–75, https://doi.org/10.1016/j.gca.2012.10.012.

O'Dogherty, L., Carter, E.S., Gorican, S., and Dumitricia, P., 2010, Triassic radiolarian biostratigraphy, *in* Lucas, S.G., ed., The Triassic Timescale: Geological Society [London] Special Publication 334, p. 163–200, https://doi.org/10.1144/SP334.8.

Ogg, J.G., and Chen, Z.-Q., 2020, The Triassic Period, *in* Gradstein, F.M., et al., eds., Geological Time Scale 2020, Volume 2: Boston, Massachusetts, Elsevier, p. 903–953, https://doi.org/10.1016/B978-0-12-824360-2.00025-5.

Prochnow, S.J., Nordt, L.C., Atchley, S.C., and Hudec, M.R., 2006, Multi-proxy paleosol evidence for Middle and Late Triassic climate trends in eastern Utah: Palaeogeography, Palaeoclimatology, Palaeoecology, v. 232, p. 53–72, https://doi.org/10.1016/j.palaeo.2005.08.011.

Retallack, G.J., and Conde, G.D., 2020, Deep time perspective on rising atmospheric CO_2: Global and Planetary Change, v. 189, p. 103177, https://doi.org/10.1016/j.gloplacha.2020.103177.

Romanek, C.S., Grossman, E.L., and Morse, J.W., 1992, Carbon isotopic fractionation in synthetic aragonite and calcite: Effects of temperature and precipitation rate: Geochimica et Cosmochimica Acta, v. 56, p. 419–430, https://doi.org/10.1016/0016-7037(92)90142-6.

Roy, S., Sanyal, P., Parthasarathi, G., Bhattacharya, S.K., and Ajay, A., 2021, Atmospheric CO_2 estimates based on Gondwanan (Indian) pedogenic carbonates reveal positive linkage with Mesozoic temperature variations: Palaeogeography, Palaeoclimatology, Palaeoecology, v. 582, 110638, https://doi.org/10.1016/j.palaeo.2021.110638.

Schaller, M.F., Wright, J.D., Kent, D.V., and Olsen, P.E., 2012, Rapid emplacement of the Central Atlantic Magmatic Province as a net sink for CO_2: Earth and Planetary Science Letters, v. 323–324, p. 27–39, https://doi.org/10.1016/j.epsl.2011.12.028.

Scotese, C.R., and Moore, T.L., 2014, Atlas of Phanerozoic Ocean Currents and Salinity (Mollweide Projection): PALEOMAP Project PaleoAtlas for ArcGIS: Evanston, Illinois, PALEOMAP Project, 26 p.

Song, H., Wignall, P.B., Tong, J., Song, H., Chen, J., Chu, D., Tian, L., Luo, M., Zong, K., Chen, Y., Lai, X., Zhang, K., and Wang, H., 2015, Integrated Sr isotope variations and global environmental changes through the late Permian to early Late Triassic: Earth and Planetary Science Letters, v. 424, p. 140–147, https://doi.org/10.1016/j.epsl.2015.05.035.

Sperling, E.A., and Ingle, J.C., Jr., 2006, A Permian-Triassic boundary section at Quinn River Crossing, northwestern Nevada, and implications for the cause of the Early Triassic chert gap on the western Pangean margin: Geological Society of America Bulletin, v. 118, p. 733–746, https://doi.org/10.1130/B25803.1.

Sun, Y., Joachimski, M.M., Wignall, P.B., Yan, C., Chen, Y., Jiang, H., Wang, L., and Lai, X., 2012, Lethally hot temperatures during the Early Triassic greenhouse: Science, v. 338, p. 366–370, https://doi.org/10.1126/science.1224126.

Svensen, H., Planke, S., Polozov, A., Schmidbauer, N., Corfu, F., Podladchikov, Y., and Jamtveit, B., 2009, Siberian gas venting and the end-Permian environmental crisis: Earth and Planetary Science Letters, v. 277, p. 490–500, https://doi.org/10.1016/j.epsl.2008.11.015.

Wang, X., Cawood, P.A., Zhao, H., Zhao, L., Grasby, S.E., Chen, Z.Q., Wignall, P.B., Lv, Z., and Han, C., 2018, Mercury anomalies across the end-Permian mass extinction in South China from shallow and deep water depositional environments: Earth and Planetary Science Letters, v. 496, p. 159–167, https://doi.org/10.1016/j.epsl.2018.05.044.

Winguth, A.M.E., Shields, C.A., and Winguth, C., 2015, Transition into a hothouse world at the Permian-Triassic boundary—A model study: Palaeogeography, Palaeoclimatology, Palaeoecology, v. 440, p. 316–327, https://doi.org/10.1016/j.palaeo.2015.09.008.

Wu, Y., Chu, D., Tong, J., Song, H., Dal Corso, J., Wignall, P.B., Song, H., Du, Y., and, Cui, Y., 2021, Six-fold increase of atmospheric CO_2 during the Permian-Triassic mass extinction: Nature Communications, v. 12, p. 2137, https://doi.org/10.1038/s41467-021-22298-7.

Zhang, L., Hay, W.W., Wang, C., and Gu, X., 2019, The evolution of latitudinal temperature gradients from the latest Cretaceous through the present: Earth-Science Reviews, v. 189, p. 147–158, https://doi.org/10.1016/j.earscirev.2019.01.025.

Printed in USA